RSC Advances

ROYAL SOCIETY OF CHEMISTRY

www.rsc.org/advances

Cite this: DOI: 10.1039/c0xx00000x

www.rsc.org/xxxxxx

ARTICLE TYPE

Electrochemical performances of cobalt oxide-carbon nanotubes electrodes via different methods as negative material for alkaline rechargeable batteries

Yanan Xu, Yanyin Dong, Xiaofeng Wang, Yijing Wang,* Lifang Jiao, Huatang Yuan and Jing Li

Received (in XXX, XXX) Xth XXXXXXXXX 20XX, Accepted Xth XXXXXXXXX 20XX
DOI: 10.1039/b000000x

Co_3O_4/CNTs samples are synthesized via different methods and investigated as negative materials for alkaline rechargeable batteries for the first time. The reasons for performance difference of those Co_3O_4/CNTs electrodes and the impact of CNTs additive amount on cycling properties are explored in detail. CNTs can remarkably enhance the electrochemical activity of Co_3O_4 materials, leading to a notable improvement of discharge capacity, cycle stability and rate capability. Co_3O_4/CNTs-C composites via the one-pot reflux method exhibit the desirable electrochemical capability. Co_3O_4/CNTs-C8 sample (mass ratio of CNTs is 8%) shows the highest discharge capacity of 526.1 mAh g^{-1}. Meanwhile, Co_3O_4/CNTs-C11 electrode (mass ratio of CNTs is 11%) displays the most outstanding cycle performance with a capacity retention rate of over 97.3 % after 200 cycles. A properly electrochemical reaction mechanism of Co_3O_4/CNTs electrode is also constructed in detail.

1. Introduction

With the rapid development of renewable and clean energy sources, safer and more efficient energy storage devices are urgently required, such as alkaline secondary batteries, lithium-ion batteries, supercapacitors and fuel cells [1-4]. Among them, alkaline secondary batteries are regarded as promising energy storage applications due to the powerful and reversible electrochemical redox reactions [5-8]. Recently, a new type alkaline rechargeable Ni/Co battery system using $Ni(OH)_2$ as cathode material and Co-based materials as anode materials was systematically proposed, which presented the outstanding discharge capacity and the environmental friendly property. It can be ascribed to the higher utilization, better electrochemical conductivity and multi-electron reaction ability of Co-based materials. The dominant surface faradaic reaction on anode electrode can be expressed as follows [9-14]:

$$Co(\mathrm{OH})_2 + 2\,\mathrm{e}^- \underset{discharge}{\overset{charge}{\rightleftharpoons}} Co + 2OH^-$$

According to the reaction, the utilization of Co is one of the most important factors influencing discharge performance of cobalt-based negative materials, which is largely dependent on the contact area between the electrode and alkaline electrolyte.

Co_3O_4 has been considered as one of the most promising electrode materials due to high capacities and multi-electron reaction ability during electrochemical reaction process [15-18]. But the poor cycle stability and rate capability limit its widespread application. Carbon materials have been proved to enhance electrochemical properties of Co-based materials by improving the dispersion, electroconductibility and utilization of active material [19, 20]. CNTs have attracted numerous research interests due to high electrical conductivity, good mechanical properties and chemically stable [21-24]. We could speculate that CNTs may be a better matrix material to modify the electrochemical performances of Co_3O_4 materials. To the best of our knowledge, there is no report on the electrochemical properties of Co_3O_4/CNTs composite as negative electrode material for Ni/Co battery.

In this paper, a series of Co_3O_4/CNTs samples are prepared by different methods and the reasons for performance difference of those electrodes are investigated in detail. The microstructure and electrochemical characteristics of Co_3O_4/CNTs composites are also explored in comparison with pure Co_3O_4 sample. And the additive amount of CNTs may have a great effect on discharge capacities and rate performances of Co-based materials. Moreover, the function mechanism is also proposed in detail.

2 Experimental

2.1 Preparation of Co_3O_4/CNTs samples

Co_3O_4 samples were synthesized via a facile reflux condensation route. The typical synthesis process was as follows: 0.14 mmol sodium citrate, 2.5 mmol $Co(NO_3)_2{\cdot}H_2O$ and 1.2 mmol hexamethylenetetramine were dissolved in 200 mL distilled water to form a homogeneous solution, respectively. Then the solution was heated to 90 ℃ and refluxed for 6 h. The resultant black solid was centrifuged and washed with water and ethanol, dried in a vacuum oven at 60 ℃ for 12 h. The sample was heated at 300 ℃ for 3 h in air atmosphere to obtain the pure Co_3O_4.

Three Co_3O_4/CNTs samples were synthesized via the following three methods: Co_3O_4/CNTs-A was prepared by simple

grinding Co_3O_4 with CNTs powder (mass ratio: 8%) for 30 min. Co_3O_4/CNTs-B was prepared by ball milling Co_3O_4 and CNTs powders in a same ratio for 10 h. Co_3O_4/CNTs-C was synthesized using the above one-pot reflux condensation route with the direct addition of CNTs. The different additive content of CNTs under mass ratio of 2%, 5%, 8% and 11% was dispersed in the homogeneous solution with ultrasonication for 2 h during the preparation process. Those Co_3O_4/CNTs-C composites with different mass ratio were designated as Co_3O_4/CNTs-C2, Co_3O_4/CNTs-C5, Co_3O_4/CNTs-C8, Co_3O_4/CNTs-C11, respectively. The CNTs content in Co_3O_4/CNTs-C8 composites is identical to the additive amount of Co_3O_4/CNTs-A sample and Co_3O_4/CNTs-B sample.

2.2. Compositional and structural characterization

The crystal structure and surface morphology of materials were characterized by X-ray diffraction (XRD, Rigaku MiniFlex Ⅱ with Cu Kα radiation), Scanning Electron Microscopy (SEM, JEOL JSM-6700F Field Emission), transmission electron microscope (TEM, JEOL JEM-2100 TEM). The elemental composition was measured by Elemental Analysis (EA, vario EL CUBE) and X-ray photoelectron spectroscopy (XPS, PHI5000 VersaProbe). The specific surface areas and porous nature of materials were further investigated by nitrogen adsorption/desorption measurements on NOVA 2200e.

2.3. Electrochemical measurements

Negative electrodes were constructed through mixing as-prepared samples with carbonyl nickel powders at a weight ratio of 1: 3. The powder mixture was pressed under 20 MPa pressure into a small pellet of 10 mm in diameter and 1.5 mm thickness. Electrochemical measurements were conducted in a three-electrode cell using a Land battery system (CT2001A). The electrolyte was 6 M KOH aqueous solution. $Ni(OH)_2$/NiOOH and Hg/HgO were used as the counter electrode and reference electrode, respectively. The obtained electrodes were charged at a current density of 200 mA g^{-1} for 3 h. After a 5 min rest, they were discharged at different current densities (100, 200, 500, 1000 mA g^{-1}) to 0.5 V (vs. Hg/HgO). Cyclicvoltammetric (CV) measurements were carried out by an electrochemical work station (CHI 660b). Electrochemical impedance spectroscopy (EIS) measurements were carried out by applying an AC voltage with 5 mV amplitude in a frequency range from 0.1 Hz to 100 kHz at open circuit potential.

3 Results and discussion

XRD patterns of CNTs, Co_3O_4 and Co_3O_4/CNTs samples synthesized via different methods were shown in Fig.1 (a). For the three Co_3O_4/CNTs composites, the major diffraction peaks are well indexed with cubic phase of Co_3O_4 (space group *Fd-3m*, JCPDS no.42-1467). An additional peak around 27° can be assigned to the characteristic peak of CNTs, and it can be clearly observed in Co_3O_4/CNTs-C sample. All the peaks of Co_3O_4 for Co_3O_4/CNTs composites are relatively broadened with the loading of CNTs, corresponding to the reduced grain size of Co_3O_4 nanoparticles. Thus the number of electrochemical active sites would be increased, thereby improving the electrochemical activity of electrode materials. X-ray photoelectron spectroscopy measurement of Co_3O_4/CNTs-C composite was performed in Fig. 1 (b). The Co 2p spectrum are best fitted by two kinds of Co species, including the Co (III) ions located at 779.5 eV and 795.2 eV, and Co (II) ions at 780.6 eV and 796.7 eV with two satellite peaks, It demonstrates the presence of both Co^{2+} and Co^{3+} species in Co_3O_4/CNTs samples[25, 26].

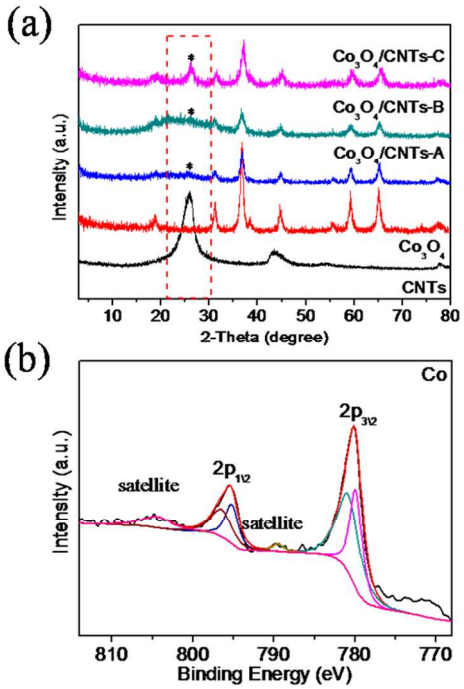

Fig. 1 (a) XRD patterns of CNTs, Co_3O_4 and Co_3O_4/CNTs samples synthesized via different methods. (b) XPS spectra of Co 2p for Co_3O_4/CNTs-C samples.

Typical TEM images in Fig. 2 were carried out to further investigate the microstructure of the obtained samples. Co_3O_4 samples are composed of numerous nanoparticles with size ranging from 5 to 20 nm in Fig. 2 (a, b). The nanoparticles are closely packed and held together as a whole, and show good crystalline nature. The starting CNTs samples (Fig.2 (c)) are formed by numerous microns long nanotubes with uniform diameter size (40-60 nm). For all the Co_3O_4/CNTs samples in Fig. 2 (d-f), CNTs can be regarded as a suitable substrate to improve dispersion state of Co_3O_4 nanoparticles. The agglomerated extent of Co_3O_4 nanoparticles in Co_3O_4/CNTs-A sample remains seriously by simply physical mixing processes. And the ball-milling disperse process also cannot alleviate the problem of agglomeration by the root for Co_3O_4/CNTs-B sample. But for Co_3O_4/CNTs-C sample, the surfaces of CNTs materials are evenly coated with numerous Co_3O_4 nanoparticles. It indicates that one-pot reflux method can effectively resolve agglomerated phenomenon and allow better dispersion of Co_3O_4 nanoparticles, compared with the physical mixture methods. The grain size of nanoparticles is reduced in a certain degree with the loading of CNTs from Fig. 3 (a, b). Clear lattice fringes for Co_3O_4 are observed in Fig. 3 (c), suggesting the crystalline nature of the particles.

Energy-dispersive X-ray spectrometry (EDS) mapping analysis in Fig. 3 (e-g) also shows that Co_3O_4 nanopaticles are well-uniform distributing on the surface of CNTs for Co_3O_4/CNTs-C sample. Furthermore, results from the EDS spectra in Fig. 3d also confirm the elemental composition of Co_3O_4/CNTs-C determined from atomic absorption spectroscopy.

The presence of Cu and Si is from the carbon-coated Cu grid.

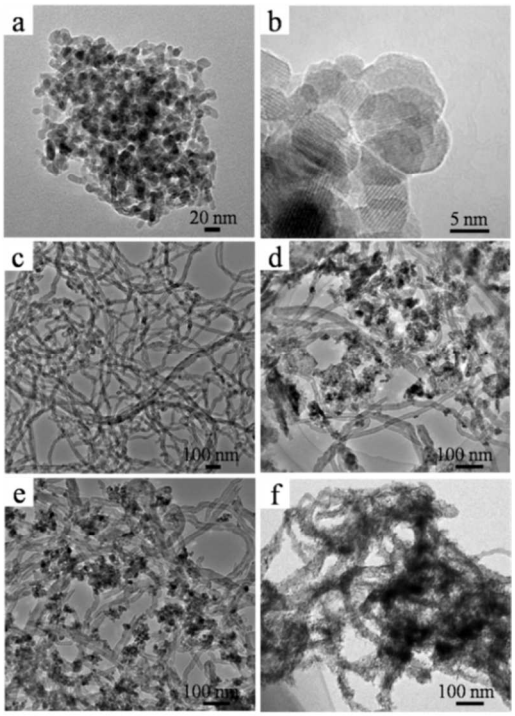

Fig. 2 TEM images of Co_3O_4 (a, b), CNTs (c), Co_3O_4/CNTs-A (d), Co_3O_4/CNTs-B (e) and Co_3O_4/CNTs-C (f) samples.

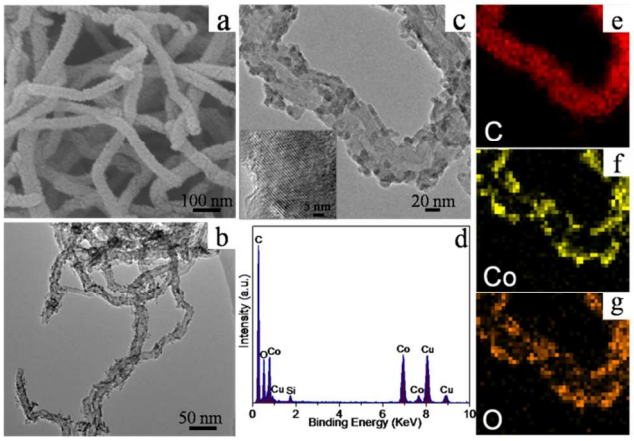

Fig. 3 SEM and TEM images (a, b, c), EDS spectrum (d) and EDS mapping results (e-g) from the Co_3O_4/CNTs-C samples.

Specific surface areas and porous nature of as-synthesized Co_3O_4 and Co_3O_4/CNTs-C sample in Fig. 4 were further investigated by Brunauer-Emmett-Teller (BET) nitrogen adsorption/desorption measurements. Based on the BET equation, the specific surface areas of Co_3O_4, Co_3O_4/CNTs-A, Co_3O_4/CNTs-B and Co_3O_4/CNTs-C samples are 82.0, 91.2, 107.4 (as shown in Fig. S1) and 164.9 m^2 g^{-1}, respectively. And pore size distributions of Co_3O_4 sample show a sharp peak at ~ 3.8 nm and a wide major peak at ~ 17.5, while only one sharp peak at ~ 3.8 nm is observed for Co_3O_4/CNTs-C samples. It shows that CNTs introduced by one-pot reflux method can effectively enhance the dispersion extent of Co_3O_4 nanoparticles with the reduced particles size. The unique features can make Co_3O_4/CNTs-C hybrid accessible to electrolytes to a larger extent, which promotes the hybrid nanocomposites as potential electrode candidates for alkaline rechargeable Ni/Co battery with high specific capacities and excellent cycling stability [27, 28].

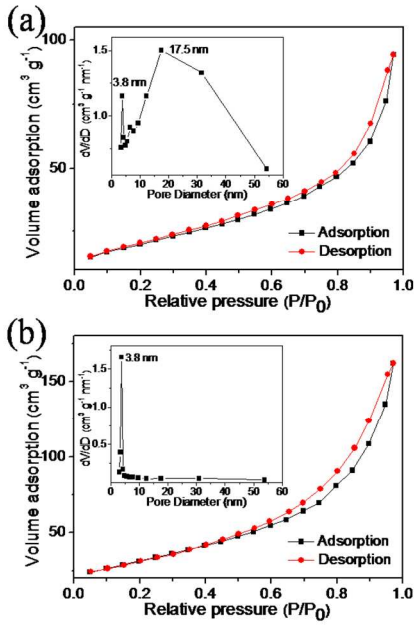

Fig. 4 Nitrogen adsorption and desorption isotherms and the pore size distribution curves of as-prepared Co_3O_4 (a) and Co_3O_4/CNTs-C (b) samples.

Cycle performances of the CNTs, pure Co_3O_4 and Co_3O_4/CNTs composites were shown in Fig. 5 (a) at a current density of 100 mA g^{-1}. CNTs can be regarded as an inactive matrix without the contribution for discharge capacities. All the electrodes need a long activation process before the intrinsic capacities are realized. Pure Co_3O_4 electrode shows the relatively low discharge capacity with the poor capacity retention rate of 47.5% after 200 cycles (S_{200}= C_{200}/C_{max}× 100%). It's worth mentioning that specific capacities and cycling stability of the three Co_3O_4/CNTs electrodes have been remarkably enhanced. It is mainly because the addition of CNTs can successfully allow good conductivity and well dispersion of Co_3O_4 nanoparticles. Meanwhile, Co_3O_4/CNTs-C electrode displays the desirable electrochemical properties as we expected. The maximum discharge capacity can reach 487 mAh g^{-1} with the capacity retention rate of 86.2 %. It is ascribed to the high specific surface areas of Co_3O_4/CNTs-C samples with the reduced particles size. The unique nanostructure can improve the dispersion of active material and enlarge the contact area between the electrode and alkaline electrolyte, compared with the physical mixture methods. Coulombic efficiency of Co_3O_4/CNTs-C materials can maintain at 76% after 30 cycles, which is significantly improved than that of Co_3O_4/CNTs-A and Co_3O_4/CNTs-B materials.

Rate capabilities of Co_3O_4/CNTs composites synthesized via different methods were measured in Fig. 5 (b). The delivered discharge capacities of Co_3O_4/CNTs-C electrode are 503, 482, 464, 438, 411 and 453 mAh g^{-1} at the different current densities of 50, 100, 200, 500, 1000 and 50 m A g^{-1} respectively, which are superior than the values of Co_3O_4/CNTs-A (416, 375, 320, 296,

244 and 314 mAh g^{-1}) and Co_3O_4/CNTs-B materials (430, 409, 378, 336, 298 and 341 mAh g^{-1}) under the same condition. These excellent data demonstrate that the Co_3O_4/CNTs-C composites are the promising alternative anode materials for alkaline secondary batteries.

To explore the influence of CNTs additive amount on cycle performance of Co_3O_4/CNTs electrodes, the related tests were also conducted in Fig.6 (a). Determined with an Element Analyzer, the measured content of CNTs in Co_3O_4/CNTs-C2, Co_3O_4/CNTs-C5, Co_3O_4/CNTs-C8 and Co_3O_4/CNTs-C11 composites is 2.15 %, 5.24 %, 7.69 % and 10.7 %, respectively. And these values are consistent with the actual mass ratios of additive CNTs in the experiments. Discharge capacities of Co_3O_4/CNTs electrodes firstly increase with the increasing content of CNTs and then decrease. These results illustrate that the appropriate amount of CNTs can lead to a remarkable enhancement of discharge capacity and cycle stability. But an excess of CNTs is not helpful to enhance the cycling properties of Co-based materials, which leads to the density decrease of active material for rechargeable Ni/Co batteries. Co_3O_4/CNTs-C8 sample shows the highest discharge capacity of 526.1 mAh g^{-1} at a current density of 100 mA g^{-1}. Meanwhile, Co_3O_4/CNTs-C11 electrode shows the most outstanding cycle performance with a capacity retention rate of over 97.3 % after 200 cycles. Results of rate performance tests also indicate that Co_3O_4/CNTs-C8 displays the most prominent discharge capacities (corresponding values are 549, 526, 519, 510, 499 and 526 mAh g^{-1}), while Co_3O_4/CNTs-C11 electrode possesses the best cycling stability.

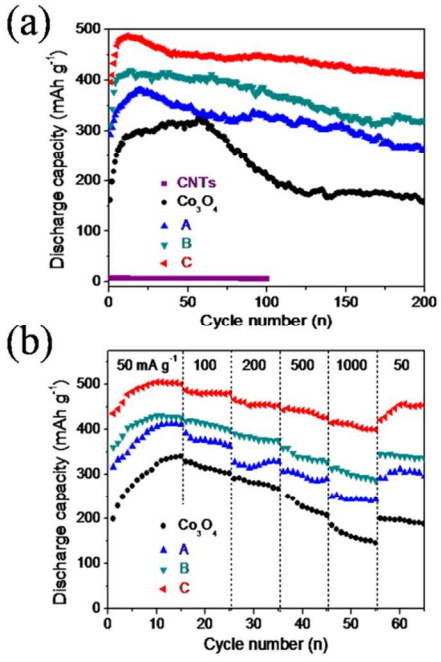

Fig. 5 Discharge capacities at a current density of 100 mA g^{-1} (a) and rate performances (b) of the CNTs, pure Co_3O_4 and Co_3O_4/CNTs samples.

In order to explain the different phenomenon of electrochemical properties, CV curves of Co_3O_4/CNT-C8 electrode for different cycles were studied in Fig. 7 (a). Only one pair of remarkable reduction-oxidation peak appears, demonstrating that most of the discharge capacities are arising from Faradaic reactions occurring on the electrode. The curve shape and peak voltage is consistent with the other Co-based materials [11, 29-31]. The reversible reaction between Co and $Co(OH)_2$ can be confirmed occurring on Co_3O_4/CNT-C electrode, suggesting that CNTs is used as a conductive substrate without electrochemical reactions. The integral area of redox peaks gradually increase, implying that discharge capacity gradually increases during charge-discharge process. The result is consistent with the measurements of cycling performance. XRD patterns of Co_3O_4/CNTs-C8 electrode at different charged/discharged state were shown in Fig. 7 (b). At fully charged state of the 1st cycle, the weakening of Co_3O_4 and the appearing of Co and $Co(OH)_2$ are clearly observed. It indicates that Co_3O_4 gradually transforms into Co and $Co(OH)_2$ during the initial charging processes. When discharged to -0.5 V, the diffraction peaks of $Co(OH)_2$ become apparent and Co_3O_4 gradually disappears. Only peaks of Co and $Co(OH)_2$ are detected after ten cycles. Compared with the charged state, the peak intensity of Co at the 10th discharged state weakens while peak intensity of $Co(OH)_2$ strengthens. It illustrates that some Co transforms to $Co(OH)_2$ during the discharge process. These results indicate that the electrochemical reaction on Co_3O_4/CNTs-C8 electrode at activation process can be summarized as follows:

Charge: $$Co_3O_4 + 4H_2O + 2e^- \rightarrow 3Co(OH)_2 + 2OH^- \quad (1)$$

$$Co(OH)_2 + 2e^- \rightarrow Co + 2OH^- \quad (2)$$

Discharge: $$Co + 2OH^- \rightarrow Co(OH)_2 + 2e^- \quad (3)$$

After activation process, charge-discharge reaction occurring on electrodes transforms into reversible redox reaction:

$$Co(OH)_2 + 2e^- \underset{discharge}{\overset{charge}{\rightleftharpoons}} Co + 2OH^- \quad (4)$$

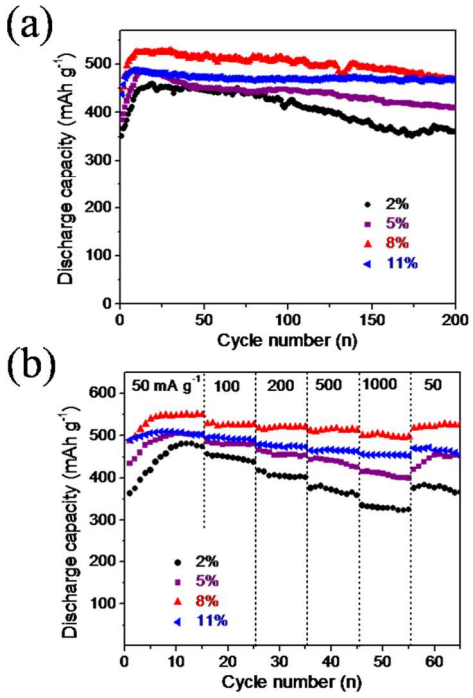

Fig. 6 Discharge capacities at a current density of 100 mA g^{-1} (a) and rate performances (d) of Co_3O_4/CNTs-C composites (different mass ratio of additive CNTs).

Charge-discharge curves of Co_3O_4/CNTs-C8 electrode at the current density of 100 mA g^{-1} further confirm the proposed mechanism in Fig. 7 (c). The charge-discharge curves of the 1st and 2nd cycle at activation process are different from other curves. It can be ascribed that Co_3O_4 gradually transforms into Co and $Co(OH)_2$ during the initial charging processes.For the 1st charged state, only a long platform at -0.98 V can be observed and it illustrates that Co_3O_4 transforms to $Co(OH)_2$ (eqn (1)) [27, 31]. But for the following cycles, two potential charge platforms in curves are observed. The first charge platform at about -0.89 V ascribes to the change from $Co(OH)_2$ to Co, corresponding to eqn (2). The other one at -1.1 V assigns to the electrolysis reaction of water. Meanwhile, only one potential platform at around -0.79 V (vs. Hg/HgO) occurs during the discharge process corresponding to eqn (3), and no changes appear in the following cycles. This fact once again reinforces that the electrochemical reaction occurring on the Co_3O_4 electrode is only reversible conversion between Co and $Co(OH)_2$ (eqn (4)) at reversible redox process.

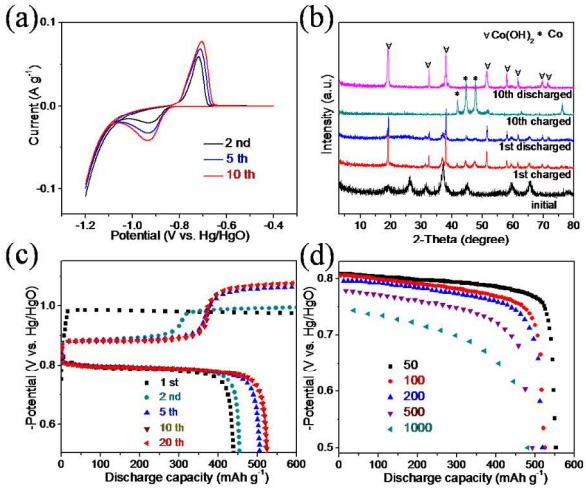

Fig. 7 CV curves (a), XRD patterns (b), charge-discharge curves at 100 mA g^{-1} (c) and different current densities (d) of Co_3O_4/CNTs-C8 composite.

CNTs in Co_3O_4/CNTs electrodes show two functions during charge-discharge processes. The addition of CNTs leads to well dispersion of active Co_3O_4 nanoparticles. Meanwhile, Co_3O_4 nanoparticles decorating by CNTs are impregnated in alkaline solution during the charge-discharge process, which can provide unobstructed pathways for OH^- transport and increase the contact area between active materials and alkaline solution. The two aspects are in favor of the electrochemical redox to enhance the capacity of Co_3O_4/CNTs electrode.

Conclusions

In summary, a series of Co_3O_4/CNTs composites are prepared by different methods for alkaline rechargeable battery and the reasons for performance difference of those electrodes are explored in detail. The one-pot reflux method (method C) can allow better dispersion of Co_3O_4 nanoparticles with the reduced size and the larger specific surface area of Co_3O_4/CNTs composites, compared with the physical mixture methods (method A, B). Electrochemical investigations also indicate that Co_3O_4/CNTs-C composites exhibit the desirable electrochemical capability. The additive amount of CNTs also has an important influence on cycling performances of Co_3O_4/CNTs-C composites. Co_3O_4/CNTs-C8 sample (mass ratio of CNTs is 8%) shows the highest discharge capacity of 526.1 mAh g^{-1}. Meanwhile, Co_3O_4/CNTs-C11 electrode (mass ratio of CNTs is 11%) displays the most outstanding cycle performance with a capacity retention rate of over 97.3 % after 200 cycles. High discharge capacities and excellent rate capability demonstrate that Co_3O_4/CNTs-C composites through one-pot reflux route are the suitable negative materials for high power applications. In addition, the faradic reaction between Co and $Co(OH)_2$ for Co_3O_4/CNTs electrode has been further investigated.

Acknowledgements

This work was financially supported by 973 (2011CB935900), NSFC (51471089), MOE (IRT13R30), 111 Project (B12015), Research Fund for the Doctoral Program of Higher Education of China (20120031110001), Tianjin Sci & Tech Project (10SYSYJC27600).

Notes and references

College of Chemistry, Collaborative Innovation Center of Chemical Science and Engineering (Tianjin), Key Laboratory of Advanced Energy Materials Chemistry (MOE), Nankai University, Tianjin 300071, P.R.China. Fax: +86 22 23503639; Tel: +86 22 23503639; E-mail: wangyj@nankai.edu.cn

‡ Footnotes should appear here. These might include comments relevant to but not central to the matter under discussion, limited experimental and spectral data, and crystallographic data.

1. F. Y. Cheng, J. Liang, Z. L. Tao and J. Chen, *Adv. Mater.*, 2011, **23**, 1695-1715.
2. V. Etacheri, R. Marom, R. Elazari, G. Salitra and D. Aurbach, *Energy Environ. Sci.*, 2011, **4**, 3243-3262.
3. Leung, X. H. Li, C. Ponce de Leon, L. Berlouis, C. T. J. Low and F. C. Walsh, *RSC Adv.*, 2012, **2**, 10125-10156.
4. M. Winter and R. J. Brodd, *Chem. Rev.*, 2004, **104**, 4245-4270.
5. R. J. Wang and Z. H. Yang, *RSC Adv.*, 2013, **3**, 19924-19928.
6. K. Vijayamohanan, T. S. Balasubramanian and A. K. Shukla, *J. Power Sources*, 1991, **34**, 269-285.
7. J. H. Huang and Z. H. Yang, *RSC Advances*, 2015, **5**, 33814-33817.
8. X. P. Gao, S. M. Yao, T. Y. Yan and Z. Zhou, *Energy Environ. Sci.*, 2009, **2**, 502-505.
9. D. S. Lu, W. S. Li, F. M. Xiao and R. H. Tang, *Electrochem. Commun.*, 2010, **12**, 362-366.
10. Y. Wang, J. M. Lee and X. Wang, *Int. J. Hydrogen Energy*, 2010, **35**, 1669-1673.
11. X. Y. Zhao, L. Q. Ma, Y. Yao, M. Yang, Y. Ding and X. D. Shen, *Electrochim. Acta*, 2010, **55**, 1169-1174.
12. S. M. Yao, K. Xi, G. R. Li and X. P. Gao, *J. Power Sources*, 2008, **184**, 657-662.
13. X. Y. Zhao, L. Q. Ma and X. D. Shen, *J. Mater. Chem.*, 2012, **22**, 277-285.
14. L. L. Jin, X. W. Li, H. Ming, H. H. Wang, Z. Y. Jia, Y. Fu, J. Adkins, Q. Zhou and J. W. Zheng, *RSC Adv.*, 2014, **4**, 6083-6089.
15. L. Wang, Z. H. Dong, Z. G. Wang, F. X. Zhang and J. Jin, *Adv. Funct. Mater.* 2013, **23**, 2758-2764.
16. C. Z. Yuan, L. Yang, L. R. Hou, L. F. Shen, X. G. Zhang and X. W. Lou, *Energy Environ. Sci.*, 2012, **5**, 7883-7887.
17. W. Sugimoto, H. Iwata, Y. Yasunaga, Y. Murakami and Y. Takasu, *Angew. Chem. Int. Ed.*, 2003, **42**, 4092-4096.
18. L. Li, Y. N. Xu, C. H. An, Y. J. Wang, L. F. Jiao and H. T. Yuan, *J. Power Sources*, 2013, **238**, 117-122.
19. Y. N. Xu, X. F. Wang, C. H. An, Y. J. Wang, L. F. Jiao and H. T. Yuan, *J. Power Sources*, 2014, **272**, 328-334.
20. F. Cai, Y. R. Kang, H. Y. Chen, M. H. Chen and Q. W. Li, *J. Mater. Chem. A*, 2014, **2**, 11509-11515.

21. Y. Liu, C. Y. Nie, X. J. Liu, X. T. Xu, Z. Sun and L. K. Pan, *RSC Adv.*, 2015, **5**, 15205-15225.
22. J. X. Li, M. Z. Zou, W. W. Wen, Y. Zhao, Y. B. Lin, L. Z. Chen, H. Lai, L. H. Guan and Z. G. Huang, *J. Mater. Chem. A*, 2014, **2**, 10257-10262.
23. H. Zhang, H. Qiao, H. Y. Wang, N. Zhou, J. J. Chen, Y. G. Tang, J. S. Li and C. H. Huang, *Nanoscale*, 2014, **6**, 10235-10242.
24. X. M. Zhai, W. Yang, M. Y. Li, G. Q. Lv, J. P. Liu and X. L. Zhang, *Carbon*, 2013, **65**, 277-286.
25. S. L. Xiong, J. S. Chen, X. W. Lou and H. C. Zeng, *Adv. Funct. Mater.*, 2012, **22**, 861-871.
26. H. M. Du, L. F. Jiao, Q. H. Wang, Q. N. Huan, L. J. Guo, Y. C. Si, Y. J. Wang and H. T. Yuan, *Cryst. Eng. Comm.*, 2013, **15**, 6101-6109.
27. D. S. Lu, W. S. Li, C. L. Tan and R. H. Zeng, *Electrochim. Acta*, 2009, **55**, 171-177.
28. Q. H. Wang, L. F. Jiao, H. M. Du, Q. T. Huan, W. X. Peng, D. W. Song, Y. J. Wang and H. T. Yuan, *Electrochim. Acta*, 2011, **56**, 4992-4995.
29. Z. W. Lu, S. M. Yao, G. R. Li, T. Y. Yan and X. P. Gao, *Electrochim. Acta*, 2008, **53**, 2369-2375.
30. L. Li, Y. P. Wang, Y. J. Wang, Y. Han, F. Y. Qiu, G. Liu, C. Yan, D. W. Song, L. F. Jiao and H. T. Yuan, *J. Power Sources*, 2011, **196**, 10758-10761.
31. S. Baskar, D. Meyrick, K. S. Ramakrishnan and M. Minakshi, *Chem. Eng. J.*, 2014, **253**, 502-507.